NANO LETTERS

pubs.acs.org/NanoLett

Probing Strain-Induced Electronic Structure Change in Graphene by Raman Spectroscopy

Mingyuan Huang,[†,§] Hugen Yan,[‡,§] Tony F. Heinz,[‡] and James Hone*[,†]

[†]Department of Mechanical Engineering and [‡]Department of Physics, Columbia University, New York, New York 10027

ABSTRACT Two-phonon Raman scattering in graphitic materials provides a distinctive approach to probing the material's electronic structure through the spectroscopy of phonons. Here we report studies of Raman scattering of the two-dimensional mode of single-layer graphene under uniaxial stress and which implicates two types of modification of the low-energy electronic structure of graphene: a deformation of the Dirac cone and its displacement away from the K point.

KEYWORDS Graphene, Raman spectroscopy, strain, electronic structure

Graphene's extremely high electron mobility,[1,2] scalability,[3,4] and excellent thermal conductivity[5] make it a promising candidate for next generation electronic devices. Because strain has been successfully utilized to modulate the band gap of single-wall carbon nanotubes,[6−8] it is natural to explore whether strain can be used to modulate the electronic structure of graphene in a useful way. In fact, recent theoretical studies predict that moderate uniform uniaxial strain shifts the Dirac cones at the K and K′ points in opposite directions,[9−11] introducing a pseudomagnetic field[12] that be used to generate structures such as electron lenses and one-dimensional (1D) channels.[13] Furthermore, inhomogeneous strain can induce a zero-field quantum Hall effect and open a band gap, a critical requirement for some applications. A second effect of strain is a reduction in the Fermi velocity; anisotropic strain should break the cylindrical symmetry of the Dirac cone.

Raman spectroscopy is a key diagnostic tool to identify single-layer graphene sheets[14] and monitor carrier density,[15,16] defects,[17] and strain.[18,19] The intervalley two-phonon mode (2D), which involves scattering of electron−hole pairs between neighboring Dirac cones, is particularly sensitive to the electronic bandstructure: changes in the separation of the Dirac points or in the electronic dispersion within each cone will alter the momentum, and therefore energy, of the 2D mode phonons. For instance, the 2D mode displays a single peak in single-layer graphene and splits into four in bilayer graphene, reflecting the evolution of the electronic structure. Therefore, to probe the effects of strain on the electronic bandstructure of graphene, we investigated the behavior of the 2D mode as a function of uniaxial strain. Because the effects of strain depend on the orientation of the graphene lattice, samples with different orientations were used, and two samples, with "zigzag" and "armchair" orientation, were studied in detail. Furthermore, because the absorption cross section is highly anisotropic,[20] the polarization of the 2D mode was studied. Finally, the excitation energy dependence of the 2D mode was used to probe the strain-induced anisotropy of the Dirac cones.

The sample fabrication method has been described previously.[19] Briefly, we mechanically deposited graphene onto a Si/SiO_2 wafer by the standard "Scotch tape" method.[21] After suitable single layer graphene flakes were identified, they were transferred onto a flexible PDMS (poly(dimethylsiloxane)) substrate. To prevent slippage, Ti strips were evaporated onto the graphene through a shadow mask. Controllable uniaxial stress was applied on the graphene by three-point bending of the substrate. Finite element analysis shows that this uniaxial stress results in roughly uniaxial strain.[19] For the Raman measurements, we employed a confocal configuration with laser wavelength of 532 nm (except for measurement of excitation energy dependence). The objective was 100× with NA = 0.95. The laser beam was linearly polarized, and the strained graphene sample could be freely rotated relative to the beam polarization.

The G mode Raman spectra, which we and others have previously studied in detail,[18,19] were used to characterize the sample orientation and calibrate the strain. The orientation of the lattice relative to the strain direction was determined by measuring the polarization of the G mode under strain; the two samples used for this study were found to have zigzag and armchair orientation (i.e., zigzag and armchair edges parallel with the strain direction, respectively), within an uncertainty of 2° (see Supporting Information). We used our previously measured values of $-12.5\ cm^{-1}/\%$ and $-5.6\ cm^{-1}/\%$ for the shift rates of the G^- and G^+ modes to calibrate the strain in the graphene. We note that there is currently disagreement in the literature about the correct values for these shift rates,[10,18,19] but the strain can be recalibrated when the shift rates are precisely confirmed.

* To whom correspondence should be addressed: e-mail, jh2228@columbia.edu; tel, 212-854-6244; fax, 212-854-3304.

§ These authors contributed equally to this work.

Received for review: 06/16/2010
Published on Web: 08/24/2010

DOI: 10.1021/nl102123c | *Nano Lett.* **2010,** *10,* 4074–4079

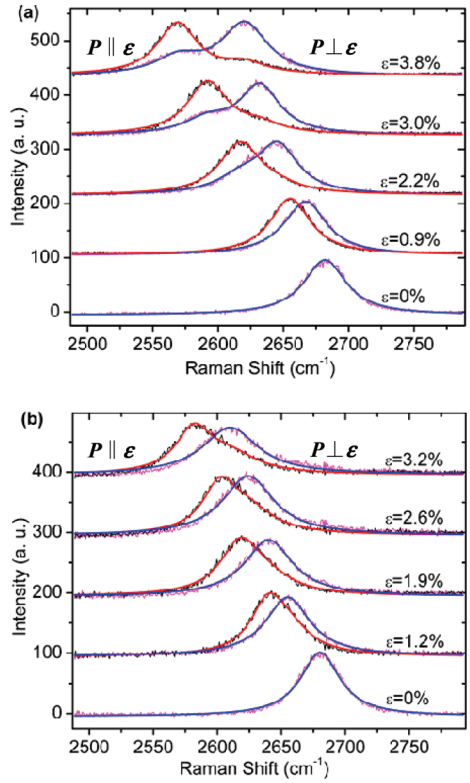

FIGURE 1. Splitting of the 2D mode of graphene under uniaxial strain. Evolution of the spectra of 2D mode of graphene, which were taken with the incident light polarization (P) parallel with (left, parallel case) and perpendicular to (right, perpendicular case) the strain axis (ε), with different strain (the background of the spectra are equally shifted and their intensities are scaled) for the zigzag sample (a) and armchair sample (b). The first spectrum from the zigzag sample and the spectra of the perpendicular case from the armchair sample are fitted by a single Lorentz peak; the other spectra are fitted by double Lorentz peaks (overlapping smooth curves).

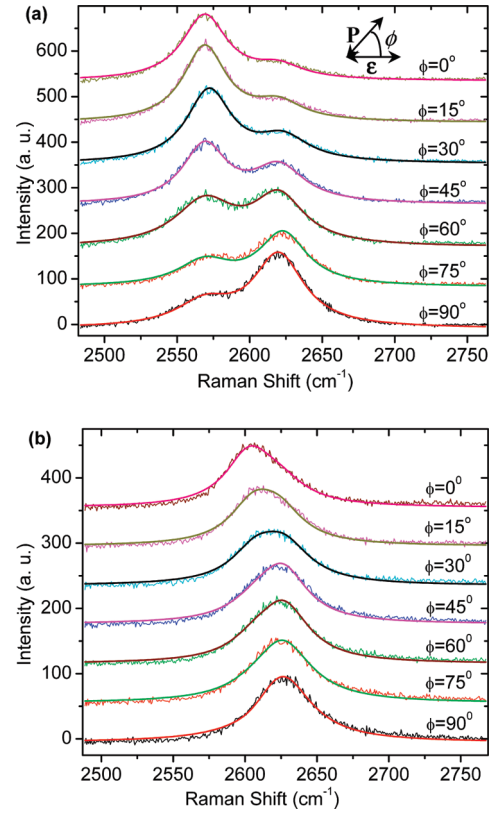

FIGURE 2. Dependence of the Raman spectra on the sample orientation. The evolution of Raman spectra of the 2D mode of graphene under constant uniaxial strain with the angle (ϕ) between the incident light polarization and the strain axis for the zigzag (a, $\varepsilon = 3.8\%$) and armchair (b, $\varepsilon = 2.6\%$) sample (The background of the spectra are equally shifted and their intensities are scaled.) The spectra are fitted by double Lorentz peaks (smooth overlapping curves).

Figure 1 shows the evolution of the spectra of the 2D mode with strain for the zigzag and armchair samples. For each strain level (except zero), two spectra were taken: one with the incident light polarization **P** parallel to the direction of the strain $\boldsymbol{\varepsilon}$ (the parallel case), and one with **P** perpendicular to $\boldsymbol{\varepsilon}$ (the perpendicular case). For the zigzag sample, each spectrum shows two distinct peaks, which we denote by $2D^+$ and $2D^-$, according to their energies. The $2D^-$ is dominant for the parallel case, and the $2D^+$ peak is dominant for the perpendicular case. However, the two cases are not symmetric: the remnant $2D^+$ peak intensity for the parallel case is smaller than that of the $2D^-$ peak in the perpendicular case. For the armchair sample, the perpendicular case displays a single symmetric peak under all strain levels; its width increases with strain, which is consistent with previous reports. However, in the parallel case under high strain, the peak shows clear asymmetry, which can be understood as partially developed splitting. Samples with intermediate (neither zigzag nor armchair) orientation showed strain-induced broadening, but not clear splitting. These results help explain why the splitting of the 2D peak has not been previously reported: it is only clear when large strain is applied along high-symmetry directions.

For the zigzag sample, the $2D^+$ and $2D^-$ shift rates are -16.3 and -29.7 cm^{-1}/%. For the armchair sample, these shift rates are -21.7 and -30.5 cm^{-1}/%. This previously undetected variation with sample orientation and light polarization could account for a good deal of the discrepancy between 2D shift rates previously reported by different groups,[9,18,19] and also indicates that measurement of the 2D mode alone is not sufficient to determine the strain state of a sample.

Next, the direction of the polarization was varied for a fixed strain in order to study the evolution of the 2D mode from the parallel case to the perpendicular case. Figure 2 shows the dependence of the 2D spectra on the angle ϕ between **P** and $\boldsymbol{\varepsilon}$ for the zigzag sample ($\varepsilon = 3.8\%$) and armchair sample ($\varepsilon = 2.6\%$). In both cases, the spectral weight shifts from the $2D^-$ peak to the $2D^+$ peak as ϕ increases from 0° to 90°, while the peak positions remain fixed. For the zigzag sample, the peak splitting is clear in all of the spectra. However, the two peaks do not evolve equally with changing ϕ: the $2D^-$ peak retains about half of its

DOI: 10.1021/nl102123c | *Nano Lett.* **2010,** *10,* 4074–4079

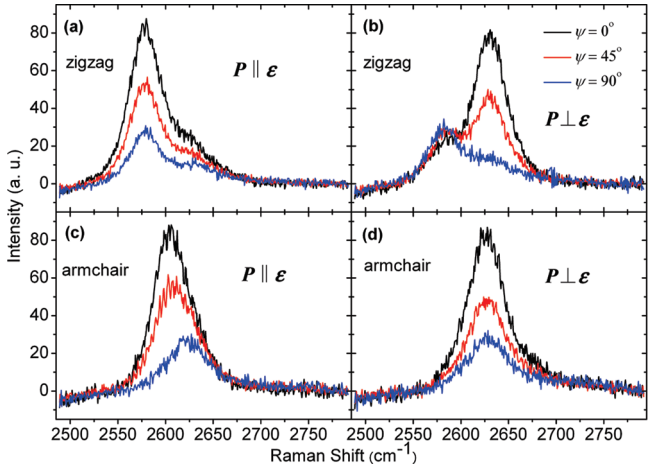

FIGURE 3. Polarization analysis of the Raman spectra of the perpendicular and parallel case for the zigzag and armchair sample. The spectra were taken with the out-going analyzer angle with respect to the incident light polarization at 0°, 45°, and 90°.

maximum intensity at $\phi = 90°$, but the $2D^+$ peak almost disappears at $\phi = 0$; the two peaks have the same intensity near $\phi = 60°$. For the armchair sample, the splitting of the 2D peak is not as obvious, due to the lower strain in the sample and the smaller splitting rate, but the frequency and shape change can be clearly observed. The $2D^-$ peak disappears at $\phi = 90°$, but the $2D^+$ peak still has about half of the maximum intensity at $\phi = 0°$; the two peaks have the same intensity near $\phi = 30°$.

The polarization of the scattered light was next studied using an analyzer. Figure 3 shows the spectra for the two samples at different angles ψ between the incident and scattered light polarization. The samples and strain levels were the same as those used above. For the parallel case of the zigzag sample (Figure 3a), the spectrum decreases in intensity with increasing ψ, but the shape remains the same, which is similar to the 2D mode from undeformed graphene.[22] However, for the perpendicular case (Figure 3b), the intensity of the $2D^+$ peak decreases with increasing ψ, nearly vanishing at $\psi = 90°$, and the intensity of the $2D^-$ peak increases (see Supporting Information for two peak fitting). As a result, the $2D^-$ peak dominates the spectrum at $\psi = 90°$ and the shape is similar to that of the parallel case. For the armchair sample, the situation is opposite: with ψ increasing, the spectra from the parallel case become similar to the perpendicular case, while the spectra from the perpendicular case retain the same shape.

We now turn to interpretation of the experimental results. In particular, we focus on the magnitude and polarization dependence of the mode splitting, which is consistent with the predicted strain-induced motion of the Dirac cones.

Figure 4a shows the basic processes involved in 2D mode Raman scattering. Although the scattering event is an instantaneous process, for the purposes of analysis it is typically broken down into the following discrete steps:[17,23−25] (i) incident light excites an electron−hole pair around a Dirac

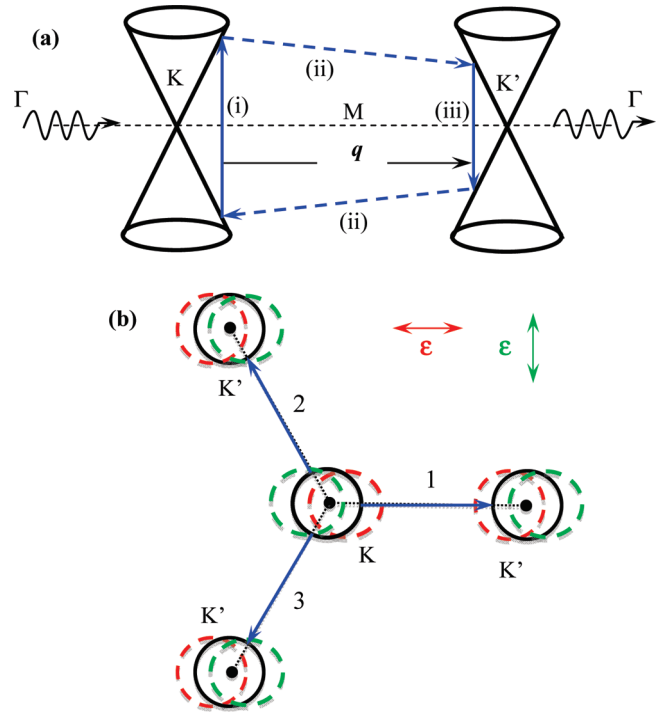

FIGURE 4. Raman scattering processes of the 2D mode in graphene. (a) Raman scattering along high symmetry direction (Γ−K−M−K′−Γ) between two nearest Dirac cones at K and K′ points associating with electronic dispersion. The scattering processes involve electron−hole pair excitation by an incoming photon (i), electron/hole inelastic scattering by phonons (ii), and electron−hole recombination and photon emission (iii). The q denotes the phonon wave vectors. (b) Three Raman scattering paths (arrows labeled by 1, 2, 3) from the Dirac cone at K point to the three nearest Dirac cones at K′ points (circles). The dashed red and green circles indicate the strain induced movement of the Dirac cone for the zigzag and armchair sample, respectively. The double headed arrows show the strain directions.

cone; (ii) the pair undergoes inelastic scattering to a neighboring Dirac cone by emitting two D mode phonons in the vicinity of the K point; (iii) the scattered pair recombines to emit a photon. From theory, the scattering in process (ii), which can occur between the Dirac cone at the K point and its three nearest neighbors at K′ points (labeled as paths 1, 2, and 3, Figure 4b), occurs mainly along high symmetry directions[26] (Γ−K), and thus involves phonons with momentum just inside (inner loop) or outside (outer loop) the K point. The observation of a single peak of the 2D mode in undeformed graphene indicates scattering through a single path, which has been attributed to the outside loop.[14,27] However, as detailed below, we find that our observations are consistent with scattering via the inside loop.

Both tight-binding and ab inito calculations predict movement of the Dirac points with strain.[11,28] An extended tight binding model[6] produces an analytical expression for the shifts; a modified version of the original theory that includes internal sublattice relaxation shows quantitative agreement with experiments on single-wall carbon nanotubes.[8] For graphene subject to uniaxial strain ε at an angle θ relative to the x axis of the crystal reference system, the modified

DOI: 10.1021/nl102123c | Nano Lett. 2010, 10, 4074–4079

tight binding model predicts a displacement of the Dirac cone from the original (unstrained) K point[6,8]

$$\Delta\vec{k} = 0.57\frac{1+\nu}{a_{C-C}}\varepsilon(\cos 2\theta\vec{i} - \sin 2\theta\vec{j}) \qquad (1)$$

where ν is the in plane Poisson ratio and a_{C-C} is the bond length. The Dirac cones at the K′ points shift opposite to those at the K points to preserve time-reversal symmetry. Figure 4b displays the displacements of the Dirac points for uniaxial strain along the zigzag and armchair directions. The displacement rate can be expressed as 60 meV/% due to the linear energy dispersion near the Dirac point.

Within this model, it is straightforward to understand the effects of strain on the 2D mode. The D mode (TO branch) phonons show a minimum in energy at the K point,[29] so a shift in a scattering path due to strain-induced Dirac point motion away from the K point will increase the corresponding 2D mode energy, while a shift toward the K point will reduce the energy. For the zigzag sample (Figure 4b), strain causes path 1 to contract, moving the path 1 phonon away from the K point and toward higher energy; paths 2 and 3 lengthen, moving the phonons toward the K point and lower energy. Therefore, path 1 gives rise to the $2D^+$ mode and paths 2 and 3 give rise to the $2D^-$ mode. For the armchair sample, path 1 lengthens and produces the $2D^-$ mode, and paths 2 and 3 contract and produce the $2D^+$ mode.

The polarization experiments allow us to verify the assignment of the specific paths to the $2D^-$ and $2D^+$ modes. The cross section to excite an electron−hole pair with the electron's (hole's) momentum $\mathbf{k}$ (measured from the Dirac point) by light with linear polarization $\mathbf{P}$ is proportional to $|\mathbf{k} \times \mathbf{P}|^2$,[20,30] so that light strongly excites electron−hole pairs with momentum of the electrons (holes) perpendicular to the polarization. The same situation occurs for light emission. Therefore polarized light can select for individual scattering paths. For instance, for the zigzag sample (Figure 4b), vertically polarized light (the perpendicular case) favors path 1 and produces the $2D^+$ peak. Likewise, the parallel case (horizontal polarization) favors paths 2 and 3, which produce the $2D^-$ peak. For the armchair sample, the behavior is reversed: the parallel case favors path 1, which produces the $2D^-$ peak, and the perpendicular case favors paths 2 and 3, which produce the $2D^+$ peak. These predictions are in agreement with the experimental data (Figure 1). Finally, we note that the results rule out significant scattering via the outside loop in Figure 4a: due to the symmetry of the TO mode around the K point, scattering via the outside loop would produce splitting in the opposite direction.

A more quantitative analysis of the behavior of the 2D peaks can be obtained by decomposing the behavior into phonon softening and electronic modulation. As discussed elsewhere,[19,31] for the phonons at (G mode) and near (2D′ mode) the Γ point, the carbon atoms vibrate along the same direction, so it follows naturally that the softening of these modes is sensitive to the strain direction. On the other hand, the TO phonon associated with the 2D mode is near the K point, where it becomes a "breathing" mode.[32] Due to its cylindrical symmetry, the softening of this mode should be much less sensitive to the direction of strain. Therefore we assume that the TO phonon softening rate $\Delta\omega_{ph}$ is orientation-independent. For the zigzag and armchair cases, the electronic change for paths 2 and 3 will be half of that of path 1, which we denote by $\Delta\omega_e$. As a consequence, the shift rates for the $2D^-$ and $2D^+$ mode of the zigzag and armchair samples can be expressed as

$$\Delta\omega_z^- = \Delta\omega_{ph} - 0.5\Delta\omega_e \quad \Delta\omega_z^+ = \Delta\omega_{ph} + \Delta\omega_e$$
$$\Delta\omega_A^- = \Delta\omega_{ph} - \Delta\omega_e \quad \Delta\omega_A^+ = \Delta\omega_{ph} + 0.5\Delta\omega_e \qquad (2)$$

Equation 2 predicts $\Delta\omega_z^+ > \Delta\omega_A^+$ and $\Delta\omega_z^- > \Delta\omega_A^-$, as observed. More quantitatively, it predicts a splitting rate of $1.5\Delta\omega_e$ for both modes. $\Delta\omega_e$ can be calculated from the shift rate of the Dirac cone: 60 meV/% × 93 cm^{-1}/eV = 5.6 cm^{-1}/%, where 93 cm^{-1}/eV is the excitation energy dispersion of the 2D mode, to give a splitting rate of 8.4 cm^{-1}/%, which is in a good agreement with the value of rate of 8.8 cm^{-1}/% measured for the armchair sample, but somewhat smaller than the value from the zigzag sample, 13.4 cm^{-1}/%. This deviation is not understood yet, but may be due to strain-induced anisotropy of the Dirac cones. Using the theoretical value for $\Delta\omega_e$, $\Delta\omega_{ph}$ is −21.9, −26.9, −24.5, and −24.9 cm^{-1}/% for the $2D^+$ and $2D^-$ modes of the zigzag and armchair sample, respectively, with an average value of −24.6 cm^{-1}/%. The good agreement between the four values indicates that the theory matches the experimental results reasonably well.

The model is also consistent with the lack clear splitting for less symmetric samples. For a general case, the 2D mode should split into three peaks which originate from the three different paths, and each peak should show different polarization properties. However, the triple peak is difficult to observe under current sample configuration due to the peak widths and the typical limit of 3−4% breaking strain in this configuration.

We now turn to the sample orientation dependence. For the zigzag sample, as discussed above, scattering path 1 produces the $2D^+$ peak and paths 2 and 3 produce the $2D^-$ peak. For an arbitrary sample orientation angle ϕ, the intensity of the Raman signal from each path is proportional to the absorption cross section: $|\mathbf{k} \times \mathbf{P}|^2$. Consequently, the intensity for the $2D^+$ and $2D^-$ peaks can be derived as

DOI: 10.1021/nl102123c | Nano Lett. 2010, 10, 4074–4079

$$\begin{cases} I_Z^{2D^+} \propto \sin^2\phi \\ I_Z^{2D^+} \propto \left(\sin^2\left(\frac{2\pi}{3}-\phi\right)+\sin^2\left(\frac{4\pi}{3}-\phi\right)\right) \end{cases} \quad (3)$$

This model shows good agreement with our experimental results (Figure 2a) (see Supporting Information). In particular, with increasing ϕ, the intensity of the $2D^+$ peak increases and that of the $2D^-$ peak decreases; the intensity of the $2D^+$ peak is suppressed at $\phi = 0°$, the $2D^+$ and $2D^-$ peaks have equal intensity at $\phi = 60°$, and the intensity of the $2D^-$ is half of that of the $2D^+$ $\phi = 90°$. Similar calculations for the armchair sample also successfully reproduce the experimental findings (see Supporting Information).

The polarization of the scattered light can be understood by considering the anisotropy of both light absorption and emission. The intensities of the $2D^+$ and $2D^-$ peaks for the zigzag sample are then

$$\begin{cases} I_Z^{2D^+} \propto \sin^2\phi\sin^2(\phi+\psi) \\ I_Z^{2D^-} \propto \left(\sin^2\left(\frac{2\pi}{3}-\phi\right)\sin^2\left(\frac{2\pi}{3}-\phi-\psi\right)+ \right. \\ \qquad \left. \sin^2\left(\frac{4\pi}{3}-\phi\right)\sin^2\left(\frac{4\pi}{3}-\phi-\psi\right)\right) \end{cases} \quad (4)$$

For the parallel case ($\phi = 0°$), the $2D^+$ peak is always suppressed and the intensity of the $2D^-$ peak decreases with increasing ψ, consistent with our experiment results (Figure 3a). For the perpendicular case ($\phi = 90°$), the intensity ratio of the $2D^+$ to $2D^-$ peak is 8:1, 4:2, and 0:3 for $\psi = 0°$, 45°, and 90°, respectively, which successfully reproduces the data shown in Figure 3b. For the armchair sample, the theoretical results also match our experimental data (see Supporting Information).

A second effect of strain on the electronic bandstructure should be a decrease in the Fermi velocity due to a reduction in the π-orbital overlap. Under uniaxial stress, the Fermi velocity should decrease along the strain axis and remain almost the same at the perpendicular direction; thus the Fermi surface should change from circular to elliptical.[11] To probe this effect, we studied the dispersive behavior of the split 2D mode for the zigzag sample at a strain level of 2.6%. The $2D^+$ and $2D^-$ modes shift linearly with laser energy, with slopes of 106 and 99 cm^{-1}/eV; the dispersion is 93 cm^{-1}/eV for the unstrained sample. (See Figure s4 in Supporting Information.) For the model described in Figure 4, the shift rate is given by

$$\frac{d\omega_{2D}}{d\omega_{laser}} = 2\frac{v_{phonon}}{v_F} \quad (5)$$

where, ω_{2D} is the Raman shift of the 2D mode, ω_{laser} is the frequency of the excitation photon, v_{phonon} is the phonon group velocity, and v_F is the Fermi velocity of the electron near the K point. The slopes of the split 2D modes are greater than that of unstrained graphene, which is consistent with a decrease in Fermi velocity with strain. Moreover, assuming that the phonon velocity is independent of the strain direction, the different dispersion of the $2D^+$ and $2D^-$ modes directly reflects the anisotropy of the Fermi velocity. The greater shift rate of the $2D^+$ mode indicates a lower Fermi velocity for electrons with wavevector parallel to the strain, as expected. We observed similar effects for the armchair and other samples. More precise measurements of the phonon band velocity under strain will permit quantitative measurement of the strain-induced change in Fermi velocity.

In a summary, the 2D Raman mode of graphene under uniaxial stress was studied systematically. For two special cases, the stress is along zigzag and armchair directions, the 2D mode splits into two distinct submodes ($2D^+$, $2D^-$), which directly reflects the strain-induced Dirac cone shifts. The intensities of the submodes show strong dependence on both incident and scattered light polarization and the sample orientation, which clearly uncovers that the submodes originate from different scattering paths. Further, the excitation energy dependence of the submodes reveals the anisotropy of the Fermi velocity of the associated electrons. In addition, our results provide new insight into the scattering process of the 2D mode.

Acknowledgment. We acknowledge support from the National Science Foundation under awards CHE-0117752 and CMMI-0927891, the New York State Office of Science, Technology, and Academic Research (NYSTAR), and the Air Force Office of Scientific Research (AFOSR) (MURI FA955009-1-0705). We thank Zheyuan Chen for experimental assistance and J. Maultzsch for helpful discussions.

Supporting Information Available. Material contains crystal orientation analysis of the sample, two-peak fitting the spectra in Figure 3b, and the theoretical analysis of the polarization of the armchair sample. This material is available free of charge via the Internet at http://pubs.acs.org.

REFERENCES AND NOTES

(1) Bolotin, K. I.; Sikes, K. J.; Jiang, Z.; Klima, M.; Fudenberg, G.; Hone, J.; Kim, P.; Stormer, H. L. *Solid State Commun.* **2008**, *146* (9−10), 351–355.
(2) Du, X.; Skachko, I.; Barker, A.; Andrei, E. Y. *Nat. Nanotechnol.* **2008**, *3* (8), 491–495.
(3) Reina, A.; Jia, X. T.; Ho, J.; Nezich, D.; Son, H. B.; Bulovic, V.; Dresselhaus, M. S.; Kong, J. *Nano Lett.* **2009**, *9* (1), 30–35.
(4) Kim, K. S.; Zhao, Y.; Jang, H.; Lee, S. Y.; Kim, J. M.; Kim, K. S.; Ahn, J. H.; Kim, P.; Choi, J. Y.; Hong, B. H. *Nature* **2009**, *457* (7230), 706–710.
(5) Balandin, A. A.; Ghosh, S.; Bao, W. Z.; Calizo, I.; Teweldebrhan, D.; Miao, F.; Lau, C. N. *Nano Lett.* **2008**, *8* (3), 902–907.
(6) Yang, L.; Han, J. *Phys. Rev. Lett.* **2000**, *85* (1), 154–157.
(7) Minot, E. D.; Yaish, Y.; Sazonova, V.; Park, J. Y.; Brink, M.; McEuen, P. L. *Phys. Rev. Lett.* **2003**, *90* (15), 156401.

DOI: 10.1021/nl102123c | *Nano Lett.* **2010,** *10,* 4074–4079

(8) Huang, M. Y.; Wu, Y.; Chandra, B.; Yan, H.; Shan, Y.; Heinz, T. F.; Hone, J. *Phys. Rev. Lett.* **2008**, *100* (13), 136803.
(9) Ni, Z. H.; Yu, T.; Lu, Y. H.; Wang, Y. Y.; Feng, Y. P.; Shen, Z. X. *ACS Nano* **2008**, *2* (11), 2301–2305.
(10) Ni, Z. H.; Yu, T.; Lu, Y. H.; Wang, Y. Y.; Feng, Y. P.; Shen, Z. X. *ACS Nano* **2009**, *3* (2), 483–483.
(11) Pereira, V. M.; Neto, A. H. C.; Peres, N. M. R. *Phys. Rev. B* **2009**, *80* (4), No. 045401.
(12) Fogler, M. M.; Guinea, F.; Katsnelson, M. I. *Phys. Rev. Lett.* **2008**, *101* (22), 226804.
(13) Pereira, V. M.; Neto, A. H. C. *Phys. Rev. Lett.* **2009**, *103* (4), No. 046801.
(14) Ferrari, A. C.; Meyer, J. C.; Scardaci, V.; Casiraghi, C.; Lazzeri, M.; Mauri, F.; Piscanec, S.; Jiang, D.; Novoselov, K. S.; Roth, S.; Geim, A. K. *Phys. Rev. Lett.* **2006**, *97* (18), 187401.
(15) Yan, J.; Zhang, Y. B.; Kim, P.; Pinczuk, A. *Phys. Rev. Lett.* **2007**, *98* (16), 166802.
(16) Pisana, S.; Lazzeri, M.; Casiraghi, C.; Novoselov, K. S.; Geim, A. K.; Ferrari, A. C.; Mauri, F. *Nat. Mater.* **2007**, *6* (3), 198–201.
(17) Ferrari, A. C. *Solid State Commun.* **2007**, *143* (1−2), 47–57.
(18) Mohiuddin, T. M. G.; Lombardo, A.; Nair, R. R.; Bonetti, A.; Savini, G.; Jalil, R.; Bonini, N.; Basko, D. M.; Galiotis, C.; Marzari, N.; Novoselov, K. S.; Geim, A. K.; Ferrari, A. C. *Phys. Rev. B* **2009**, *79* (20), 205433.
(19) Huang, M. Y.; Yan, H. G.; Chen, C. Y.; Song, D. H.; Heinz, T. F.; Hone, J. *Proc. Natl. Acad. Sci. U.S.A.* **2009**, *106* (18), 7304–7308.
(20) Gruneis, A.; Saito, R.; Samsonidze, G. G.; Kimura, T.; Pimenta, M. A.; Jorio, A.; Souza, A. G.; Dresselhaus, G.; Dresselhaus, M. S. *Phys. Rev. B* **2003**, *67* (16), 165402.
(21) Novoselov, K. S.; Geim, A. K.; Morozov, S. V.; Jiang, D.; Zhang, Y.; Dubonos, S. V.; Grigorieva, I. V.; Firsov, A. A. *Science* **2004**, *306* (5296), 666–669.
(22) Yoon, D.; Moon, H.; Son, Y. W.; Samsonidze, G.; Park, B. H.; Kim, J. B.; Lee, Y.; Cheong, H. *Nano Lett.* **2008**, *8* (12), 4270–4274.
(23) Thomsen, C.; Reich, S. *Phys. Rev. Lett.* **2000**, *85* (24), 5214–5217.
(24) Basko, D. M. *Phys. Rev. B* **2008**, *78* (12), 125418.
(25) Basko, D. M.; Piscanec, S.; Ferrari, A. C. *Phys. Rev. B* **2009**, *80* (16), 165413.
(26) Maultzsch, J.; Reich, S.; Thomsen, C. *Phys. Rev. B* **2004**, *70* (15), 155403.
(27) Kurti, J.; Zolyomi, V.; Gruneis, A.; Kuzmany, H. *Phys. Rev. B* **2002**, *65* (16), 165433.
(28) Mohr, M.; Papagelis, K.; Maultzsch, J.; Thomsen, C. *Phys. Rev. B* **2009**, *80* (20), 205410.
(29) Maultzsch, J.; Reich, S.; Thomsen, C.; Requardt, H.; Ordejon, P. *Phys. Rev. Lett.* **2004**, *92* (7), No. 075501.
(30) Cancado, L. G.; Pimenta, M. A.; Neves, B. R. A.; Medeiros-Ribeiro, G.; Enoki, T.; Kobayashi, Y.; Takai, K.; Fukui, K.; Dresselhaus, M. S.; Saito, R.; Jorio, A. *Phys. Rev. Lett.* **2004**, *93* (4), No. 047403.
(31) Yan, H. G.; Huang, M. Y.; Hone, J.; Heinz, T. F. To be published.
(32) Tuinstra, F.; Koenig, J. L. *J. Chem. Phys.* **1970**, *53* (3), 1126–1130.

DOI: 10.1021/nl102123c | *Nano Lett.* **2010,** *10,* 4074–-4079